Journal of ELECTRONIC MATERIALS
https://doi.org/10.1007/s11664-018-6802-8
© 2018 The Minerals, Metals & Materials Society

# Thermal Annealing Effects on the Electrical and Structural Properties of Ni/Pt Schottky Contacts on the Quaternary AlInGaN Epilayer

ENGIN ARSLAN,[1,2,5,6] ŞEMSETTIN ALTINDAL,[3] SERTAÇ URAL,[2] ÖMER A. KAYAL,[2] MUSTAFA ÖZTÜRK,[2] and EKMEL ÖZBAY[2,4]

1.—Department of Electrical and Electronics Engineering, Antalya Bilim University, 07190 Antalya, Turkey. 2.—Nanotechnology Research Center-NANOTAM, Bilkent University, 06800 Ankara, Turkey. 3.—Department of Physics, Faculty of Science and Arts, Gazi University, Teknikokullar, 06500 Ankara, Turkey. 4.—Department of Physics, Department of Electrical and Electronics Engineering, Bilkent University, 06800 Ankara, Turkey. 5.—e-mail: engina@bilkent.edu.tr. 6.—e-mail: engin.arslan@antalya.edu.tr

Pt/Au, Ni/Au, Ni/Pt/Au Schottky contacts were placed on a quaternary $Al_{0.84}In_{0.13}Ga_{0.03}N$ epilayer. The electrical and structural properties of the as-deposited Pt/Au, Ni/Au, Ni/Pt/Au and annealed Ni/Pt/Au Schottky contacts were investigated as a function of annealing temperature using current–voltage (*I–V*), capacitance–voltage (*C–V*), and high resolution x-ray diffraction measurements (HR-XRD). According to the *I–V*, Norde, and *C–V* methods, the highest Schottky barrier height (SBH) was obtained for the Pt/Au (0.82 eV (*I–V*), 0.83 eV (Norde), and 1.09 eV (*C–V*)) contacts when they were compared with the other as-deposited Schottky contacts. The estimated SBH of the annealed Ni/Pt/Au Schottky contacts, calculated from the *I–V* results, were 0.80 eV, 0.79 eV, and 0.78 eV at 300°C, 400°C, and 500°C, respectively. The SBH decreases with an increase in the annealing temperature up to 500°C compared with that of the as-deposited Ni/Pt/Au Schottky contact. The observed extra peaks in the annealed samples confirm the formation of a new interfacial phase at the interface. However, the diffraction patterns of the annealed Schottky contacts did not change as a function of the annealing temperature. The higher ideality factors values were obtained for as-deposited Pt/Au (5.69), Ni/Au (6.09), and Ni/Pt/Au (6.42) Schottky contacts and annealed Ni/Pt/Au (6.42) Schottky contacts at 300°C (6.89), 400°C (7.43), and 500°C (8.04). The higher *n* results can be attributed to current-transport mechanisms other than thermionic emission, such as dislocation related tunneling.

**Key words:** B1. AlInGaN, A1. Schottky, A3. metalorganic chemical vapor deposition (MOCVD), annealing effects

## INTRODUCTION

In the last decade, wurtzite group III-nitride semiconductors have attracted considerable interest due to their strong potential for applications in high-power, high-frequency electronic device applications, and also in optical devices.[1–6] The ternary alloys, such as AlGaN, AlInN, InGaN, and quaternary AlInGaN alloy, have become promising candidates because of their applicatility to several types of device structures, high frequency and high power devices, light emitting diodes (LED), and laser diodes (LD).[4–7]

In the last few years, because of its versatility in adjusting material properties, i.e. lattice constant and energy bandgap, separately, quaternary AlInGaN has become the focus of interest.[6–9] The independent

(Received July 10, 2018; accepted November 8, 2018)

Published online: 15 November 2018

control properties of the lattice constant and energy band gap, by varying the indium (In) and aluminum (Al) compositions of the AlInGaN alloys, also provide additional freedom to adjust the strain and band gap, and make them attractive materials as active layers in visible and ultraviolet (UV) LED and LD.[6–9] In addition, the spontaneous and piezoelectric polarization field in a pseudomorphically grown AlInGaN epilayer on a GaN template layer can be controlled by changing the In and Al composition of the AlInGaN epilayer that is used as a barrier layer in high electron mobility transistor (HEMT) structures.[7–9] This property is an important opportunity for the growth of the high sheet carrier density of GaN-based HEMT. On the other hand, In and Al ratio-dependent lattice constant regulation can be used for the growth of HEMT with a lattice-matched barrier and GaN template layer with an appropriate In and Al ratio.[8,9] These properties offer an important opportunity in the realization of the depletion mode (d-mode) and enhancement-mode (e-mode) operations in GaN based HEMTs.[9] Recently, a GaN-based HEMT with quaternary AlInGaN alloy barrier has been demonstrated with promising performance in comparison with the AlGaN and AlInN barrier HEMT, which demonstrated the high potential of quaternary AlInGaN alloy in the high-power, high-frequency field.[8,9]

Schottky contacts are the important part of HEMT when used as a gate contactor or for other device applications. Low leakage current and good thermal stability play main roles in many electronic and optoelectronic devices.[10–13] However, abnormal leakage currents under reverse bias strongly degrade the gate current characteristics and increase power consumption,[10–12] hence the need for a high quality Schottky contact to the GaN-based HEMT. Because of high defect and dislocation densities in the GaN-based materials, high leakage currents were measured via the defects of dislocation tunneling.[14,39,41] A large SBH has been shown to decrease leakage currents and thus improve the noise level and the high voltage performance of the device.[11,13–16] Schottky contacts on GaN-based structures need a high SBH. To date, in order to reduce the reverse-biased leakage current in Schottky contacts, incorporating a Schottky metal possessing high work function, such as Au (5.1 eV), Pd (5.12 eV), Ni (5.15 eV), or Pt (5.65 eV), is a common method of maximizing the effective SBH of the metal/n-GaN, metal/AlInN/GaN, or metal/AlGaN/GaN HEMT contacts.[17–22] However, these studies are not enough for high quality Schottky contacts on GaN-based materials. Further improvement should be done. Therefore, various rare metals, alloys, and multilayer systems have also been investigated and the thermal annealing of the Schottky contacts, in particular, has been reported to be quite effective in some cases.[23–30] Khanna et al.[23] investigated the temperature dependence of $W_2B_5$-based rectifying contacts to n-GaN and showed that the SBH (0.65 eV) increased with annealing temperature up to 200°C. Reddy et al.[24] investigated the thermal annealing temperature effects on the electrical and structural properties of Pt/Mo Schottky contacts on *n*-type GaN. They concluded that Pt/Mo contact does not seriously suffer from thermal degradation during the annealing process, even at 600°C. On the other hand, Wang et al.[25] reported the degradation of Pt contacts on n-GaN above 600°C. Order et al.[26] studied the electrical properties and thermal stability of $ZrB_2$ Schottky contacts to n-GaN and reported a barrier height of 0.80 eV, as-deposited. However, after annealing in a nitrogen atmosphere for 20 min., the barrier height decreased to 0.70 eV at 300°C and 0.60 eV at 400°C. Miura et al.[27] investigated the thermal annealing effects on Ni/Au Schottky contact diodes on n-GaN and AlGaN/GaN HEMT structures. They found that the most suitable metals for this system are Pt and Ir, after annealing at 500°C. They also characterized the Schottky contacts with and without Ni metal and it was found to play a significant role in the Ni/Pt(Ir)/Au system in obtaining better quality Schottky contacts. In their study, they applied the Ni/Pt(Ir)/Au system as a gate electrode in the AlGaN/GaN HEMTs, and they obtained decrements in gate leakage current as well as increments in drain breakdown voltage without degrading the transconductance of the transistor.

The improvement of the current-transport properties of Schottky contacts on the quaternary AlInGaN alloy is also very important for the AlInGaN/GaN HEMTs and/or other quaternary AlInGaN alloy-based device applications. Unfortunately, few studies can be found about the current-transport properties of Schottky contacts on the quaternary AlInGaN alloy in the literature.[31–33]

Although extensive studies on the annealing effect on the current-transport mechanisms of the Schottky contacts on GaN[16,18,23–29] and AlGaN[18,19,27,30] have been performed, very little information is available concerning the annealing effect on the properties of Schottky contacts on the quaternary AlInGaN alloy.[34] The thermal annealing treatment effects on the Pt-$Al_{0.08}In_{0.08}Ga_{0.84}N$ Schottky contacts at various temperatures (300–600°C) have been reported by Ghazai et al.[34] They conclude that high SBH and better surface morphology were obtained for Pt-$Al_{0.08}In_{0.08}Ga_{0.84}N$ Schottky contacts annealed at 400°C.

This study investigates the current-transport mechanisms of the Pt/Au, Ni/Au, and Ni/Pt/Au Schottky contacts on the MOCVD-grown quaternary $Al_{0.84}In_{0.13}Ga_{0.03}N$ epilayers grown on a GaN/$Al_2O_3$ structure. In the second part, the thermal annealing effects on the current-transport mechanism of the Ni/Pt/Au Schottky contacts are presented as a function of the annealing temperature.

## EXPERIMENTAL PROCEDURE

The nominally 118 nm $Al_xIn_yGa_{1-x-y}N$ epilayers were grown on a GaN/$Al_2O_3$ structure in a low-pressure metalorganic chemical vapor deposition

(MOCVD) reactor (Aixtron 200/4 HT-S) using triethylgallium (TEGa), trimethylaluminum (TMAl), trimethylindium (TMIn), and ammonia as Ga, Al, In, and N precursors, respectively. In the growth process, a c-plane (0001) double-polished 2-inch diameter $Al_2O_3$ substrate was used. The surface of the $Al_2O_3$ substrate was baked under $H_2$ ambient at 1200°C for 10 min. After the cleaning process, a nominally 50 nm thick, low-temperature GaN nucleation layer was grown at a temperature of 515°C. The growth process was continued with the growth of the GaN template layer, which contains two parts at different growth conditions. The thickness of the first part of the GaN template layer is 1 $\mu$m and is grown at 1040°C and 300 mbar pressure. The second part of the GaN template layer, a nominally 2 $\mu$m thick undoped GaN layer, was grown at a temperature of 1060°C and a pressure of 150 mbar. The GaN template layer was followed by 118 nm thick quaternary $Al_xIn_yGa_{1-x-y}N$ epilayers that were grown at a temperature of 1150°C and 30 mbar (Fig. 1a). The thickness of the $Al_xIn_yGa_{1-x-y}N$ epilayers was determined from the focused ion beam (FIB) image of the samples (Fig. 1b).

Before device processing, molar fractions of the indium and the aluminum in the $Al_xIn_yGa_{1-x-y}N$ epilayers were determined by x-ray diffraction (XRD) and x-ray photoelectron spectroscopy (XPS).

After the characterization process, wafers were cut into several pieces of 8 × 8 mm. Square Van Der Pauw shape ohmic contacts and 1 mm diameter circular dot Schottky contacts were formed on the samples (Fig. 1a). Prior to the metallization process, six samples were selected. Before ohmic contact formation, all of the six samples were cleaned with acetone in an ultrasonic bath. Then, each sample was treated with isopropyl alcohol and rinsed in deionized (DI) water that possessed 18 MΩ resistivity. After cleaning, the samples were dipped in a solution of $HCl:H_2O$ (1:1) for 30 s in order to remove the surface oxides, and were then rinsed in DI water again for a prolonged period.

The Ti/Al/Ni/Au (45/120/55/300 nm) metals were deposited on the AlInGaN surface under a vacuum of $10^{-7}$ Torr and were annealed at 800°C for 45 s in $N_2$ ambient in order to form the ohmic contact. The same ohmic contact recipe was applied for all of the six samples. After the formation of the ohmic contacts, room temperature Hall measurements were done for all samples. Hall measurements were continued by Schottky contact formation. The Pt/Au (40/250 nm), Ni/Au (40/250 nm), and Ni/Pt/Au (30/40/250 nm) (done on 4 samples) Schottky contacts were formed by evaporation. In order to study the thermal annealing effects on the current-transport mechanism of Ni/Pt/Au Schottky contacts on quaternary $Al_xIn_yGa_{1-x-y}N$ epilayers, samples were annealed at a temperature of 300°C, 400°C, and 500°C for 2 min in an $N_2$ atmosphere in rapid thermal annealing (RTA) equipment.

The XRD measurements were performed by using a Rigaku Smart Lab high-resolution diffractometer system, delivering CuK$\alpha$1(1.544 Å) radiation. A Thermo Scientific K-$\alpha$ XPS system was used for XPS measurement. The room temperature capacitance–voltage ($C$–$V$) and conductance–voltage ($G/\omega$–$V$) measurements of the samples were performed by an HP 4192A LF impedance analyzer at 500 kHz. The measurements were performed under the test signal of 50 mV peak to peak. The resolution of capacitance and conductance measurements was

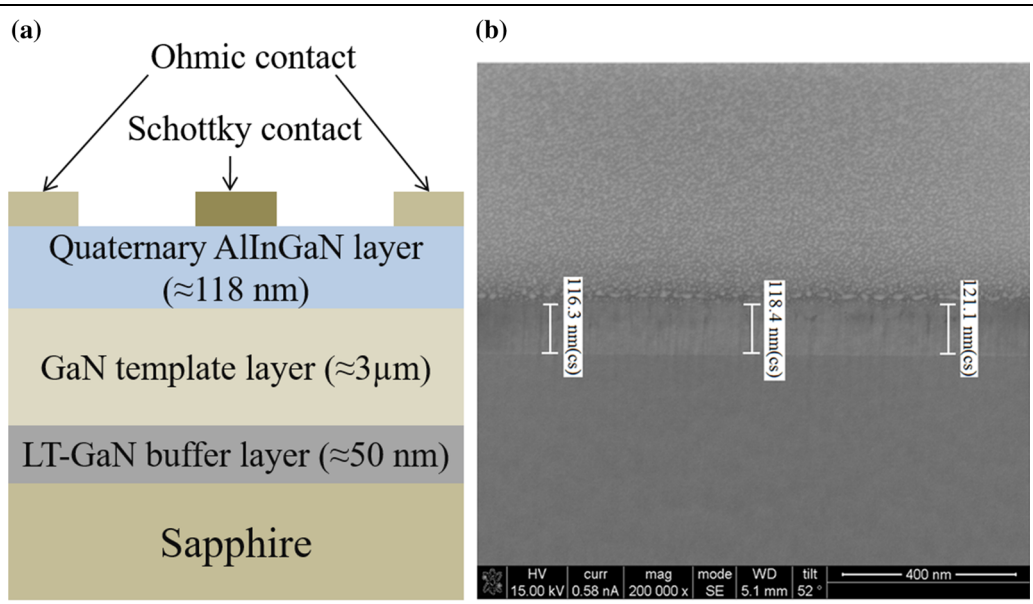


Fig. 1. (a) Schematic diagram of the quaternary $Al_{0.84}In_{0.13}Ga_{0.03}N$ epilayer grown on GaN/sapphire structures, (b) cross-section FIB image of the quaternary $Al_{0.84}In_{0.13}Ga_{0.03}N$ epilayer on the GaN/sapphire structures ($Al_{0.84}In_{0.13}Ga_{0.03}N$ epilayer thickness was determined from FIB image).

± 0.4 pF. The current–voltage (*I–V*) characteristics of the samples were measured with a Keithley model 199 dmm/scanner. The resolution of current measurements was ± 1 nA. The temperature of the samples was measured with a Lake Shore model 321 auto-tuning temperature controller with sensitivity better than ± 0.1 K. Moreover, the carrier mobility and the carrier density were measured using the Hall Measurement System in the temperature range of 12–300 K. The surface morphology characterizations of the quaternary $Al_xIn_yGa_{1-x-y}N$ epilayers were also done by atomic force microscopy (AFM) in contact mode with a commercial VEECO CPII.

## RESULTS AND DISCUSSION

In order to assess the surface quality of the $Al_xIn_yGa_{1-x-y}N$ epilayers grown on GaN/sapphire structures under optimized growth parameters, the surface morphology of the samples was observed by optical microscopy and AFM imaging was done over a $4.5 \times 4.5\ \mu m^2$ scan size. The surface of the AlInGaN epilayers has a crack-free and mirror-like surface morphology. Figure 2 shows the AFM imaging of the epilayers grown on GaN/sapphire structures. It can be seen that the sample has a smooth surface morphology with low roughness (RMS = 0.63 nm) and low defect density.

XRD analyses were performed to investigate the phase and crystalline quality of the quaternary AlInGaN layer. The $\omega$-$2\theta$ scans for the $Al_xIn_yGa_{1-x-y}N$/GaN/sapphire structures are shown in Fig. 3. The spectra reveal a (002) plane peak of the GaN layer at 34.915°. Besides the (002) diffraction peak of GaN, the diffraction from $Al_xIn_yGa_{1-x-y}N$ epilayers was also observed at a higher angle side of GaN (002) diffraction peak at 35.926°.

The full width at half maximum (FWHM) of the rocking curve ($\omega$-scan), a measure for the mosaicity in an AlInGaN epitaxial layer, is commonly used to quantify its crystal structure. The structural quality of the AlInGaN layers was estimated through XRD $\omega$-scans. The FWHM values of the x-ray rocking curve are 317 arcsec and 500 arcsec for the (002) and (102) planes, respectively. These results confirm that the layers are grown without being affected macroscopically by phase separation and have a wurtzite crystal structure with high crystalline quality, as indicated by the FWHM of the symmetric and asymmetric planes.

The In and Al molar fraction in the $Al_xIn_yGa_{1-x-y}N$ epilayers were estimated using x-ray photoelectron spectroscopy (XPS) and verified by HR-XRD. The aluminum, indium, and gallium incorporations of the sample were found to be approximately 84% (Al), 13% (In) and 3% (Ga), respectively. The Al and In compositions were determined by the simulation fitting of $2\theta$-scans at an AlInGaN (0002) diffraction pattern using the Global Fit software (Fig. 3). XPS measurement was used to confirm the Al and In content in the AlInGaN layers.

In order to measure the carrier density and the mobility of quaternary AlInGaN alloy, Hall measurements were carried out between 10 K and 300 K at a magnetic field of 0.5 T using square Van der Pauw geometry. The temperature-dependent low magnetic field Hall (0.5 T) mobility and carrier density versus temperature curves are given in Fig. 4. The sign of the Hall voltage showed that the *n*-type carriers determine the current conductions in the unintentionally doped quaternary $Al_{0.84}In_{0.13}Ga_{0.03}N$ epilayer.

Figure 4 shows temperature-dependent Hall Effect measurement results for the sample before Schottky contact formation. The results indicate that at $T = 300$, K the electron Hall mobility is 450 $cm^2\ V^{-1}\ s^{-1}$; it increases monotonically with decreasing temperature from room temperature, begins to level off at about 60 K and saturates at about 50 K (Fig. 4). At $t = 12$ K, its value equals 876 $cm^2\ V^{-1}\ s^{-1}$. This behavior reflects the 2-dimensional (2D) character of the electrons in the channel between the AlInGaN layer and GaN layer. The carrier density has no temperature dependence between the temperature ranges of 12–60 K. At higher temperatures, the carrier density increases

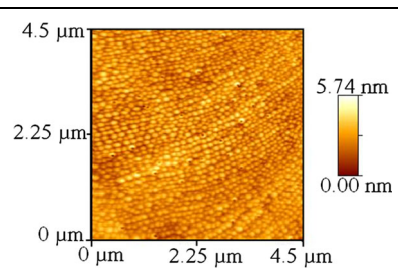


Fig. 2. AFM images ($4.5 \times 4.5\ \mu m^2$ scans) of the nominally 118 nm thick quaternary $Al_{0.84}In_{0.13}Ga_{0.03}N$ epilayer grown on GaN/sapphire structures.

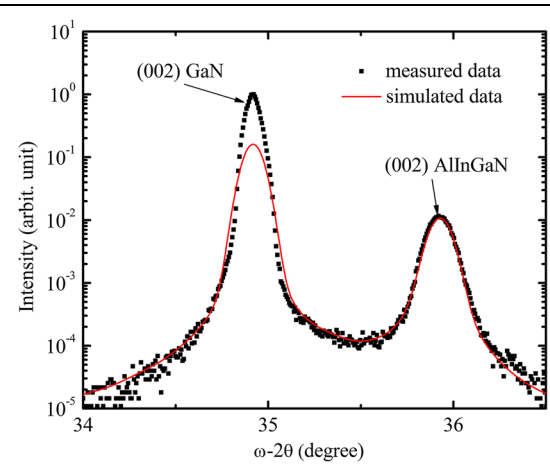


Fig. 3. The XRD $\omega - 2\theta$ scans of the quaternary $Al_{0.84}In_{0.13}Ga_{0.03}N$ epilayer grown on GaN/sapphire structures and simulation of the measured curve by GlobalFit software.

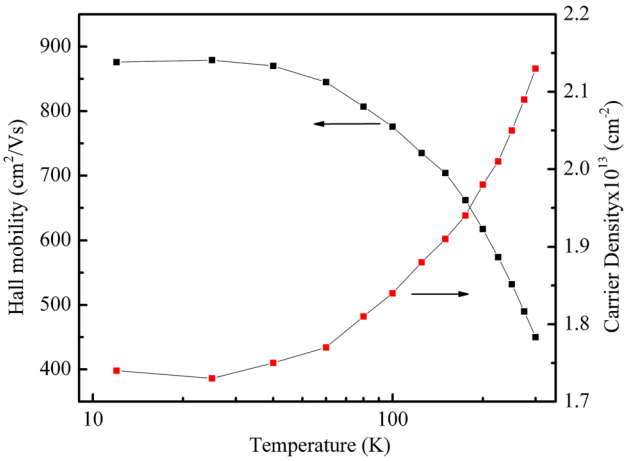


Fig. 4. Temperature-dependent Hall measurement results for the quaternary $Al_{0.84}In_{0.13}Ga_{0.03}N$ epilayer grown on GaN/sapphire structures from 12 K to 300 K. The line was used for the eye guide.

monotonically with increasing temperature and approaches values of $2.13 \times 10^{13}$ cm$^{-2}$ at 300 K.

X-ray powder diffraction measurements were done to identify the interfacial reaction products that occur between the Ni/Pt/Au Schottky contacts and AlInGaN epilayer before and after the annealing process. Figure 5 shows the XRD $2\theta$-scan patterns of the Ni/Pt/Au Schottky contacts before and after annealing at 300°C, 400°C, and 500°C, respectively. Figure 5a shows the XRD plot of the as-deposited Ni/Pt/Au Schottky contact on the AlInGaN epilayer. As can be seen in the figure, in addition to the characteristic peaks of GaN (002), (004), and AlInGaN (002), there are peaks that come from the Pt, Ni, and Au metals. Figure 5a, b, c, and d shows the XRD $2\theta$ patterns of the as-deposited Ni/Pt/Au Schottky contacts and after annealing at 300°C, 400°C, and 500°C, respectively. In addition to peaks that are observed in the as-deposited contacts, there are other extra peaks observed in the annealed samples. This indicates formation of a new interfacial phase at the interface. However, the diffraction patterns of the annealed Schottky contacts did not change as a function of the annealing temperature. This means all of the annealing temperatures created same interfacial crystal phase.

The performance of Schottky contacts usually depends on the properties of the semiconductor surface, native, or deposited interfacial layer between semiconductor and metals, number of donor or acceptor atoms, and surface/interface states ($N_{ss}$), which have strongly affected the ideality factor and Schottky barrier height.[35–38]

Figure 6a shows the semi-logarithmic plots of forward and reverse $I$–$V$ characteristics of the as-deposited Pt/Au, Ni/Au, Ni/Pt/Au Schottky contacts and Ni/Pt/Au Schottky contacts, annealed at 300°C, 400°C, and 500°C, on quaternary AlInGaN epilayer measured at room temperature. As shown in this figure, all these plots exhibit the typical behavior of a diode with a good rectifying behavior. In the intermediate bias region, ln $I$ versus $V$ plots show a linear behavior, but they start to deviate from the linearity especially due to the effects of $R_s$. In addition, the observation of none or soft saturating behavior in the reverse-bias region suggest that the SBH is a function of applied bias voltage. In Schottky type contacts, SBH, $n$ and $R_s$ are Schottky contact properties which govern current-transport/conduction by thermionic-emission (TE) theory.

The more important Scottky contact parameters, SBH and $n$, can be extracted by the linear fitting of the ln $I$ versus $V$ plots in the intermediate bias region (≥ 3kT/q) using standard TE theory. According to TE theory, in this region, the relationship between $I$ and $V$ can be expressed with an equation given below[38,39];

$$I = AA^{*}T^{2}\exp\left(-\frac{q\Phi_{B0}}{kT}\right)\left[\exp\left(\frac{q(V-IR_s)}{nkT}\right)-1\right] \tag{1}$$

In the Eq. 1 $A^*$ is the effective Richardson constant ($A^*$) and were calculated using $A^* = 4\pi m^* q k^2/h^3$ relation, where $m^*$ is effective electron mass for quaternary $Al_{0.84}In_{0.13}Ga_{0.03}N$ epitaxial layer and were estimated that $m^* = 0.34m_0$ by a linear extrapolation from the measured values of AlN, InN, and GaN.[40] Thus, the Richardson constant can be calculated to be 41.2 A cm$^{-2}$ K$^{-2}$. In the equation, $q$ is electron charge, $k$ is the Boltzmann constant and $h$ is the Planck constant. The other terms in Eq. 1 of $\Phi_{B0}$, $R_s$, $n$ and $A$ are the Schottky barrier height, series resistance, ideality factor, and contact area, respectively.[37]

The terms before the square brackets constitute the reverse-saturation current ($I_s$) that is obtained from the intercept of the linear regime of the ln $I$–$V$ plot, but the value of $n$ is obtained from the slope of this plot using Eq. 2a:

$$n = \frac{q}{kT}\left[\frac{\mathrm{d}(V-IR_s)}{\mathrm{d}(\ln I)}\right] \tag{2a}$$

Moreover, a Schottky contact parameter of $\Phi_{B0}$ can be calculated by using the diode area and calculated $I_s$ in Eq. 2b.[37,39]

$$\Phi_{B0} = \frac{kT}{q}\ln\left(\frac{AA^{*}T^{2}}{I_s}\right) \tag{2b}$$

The values of $I_s$, $n$ and $\Phi_{B0}$ parameters are given in Table I for each contact. The value of SBH obtained from the reverse bias capacitance–voltage ($C$–$V$) characteristics is higher than that of SBH obtained from the forward bias current–voltage ($I$–$V$) characteristics for each diode, due to the nature of the measurement method.[37] According to $I$–$V$, Norde, and $C$–$V$ methods, the highest SBH (0.82 eV) was obtained for the as-deposited Pt/Au Schottky

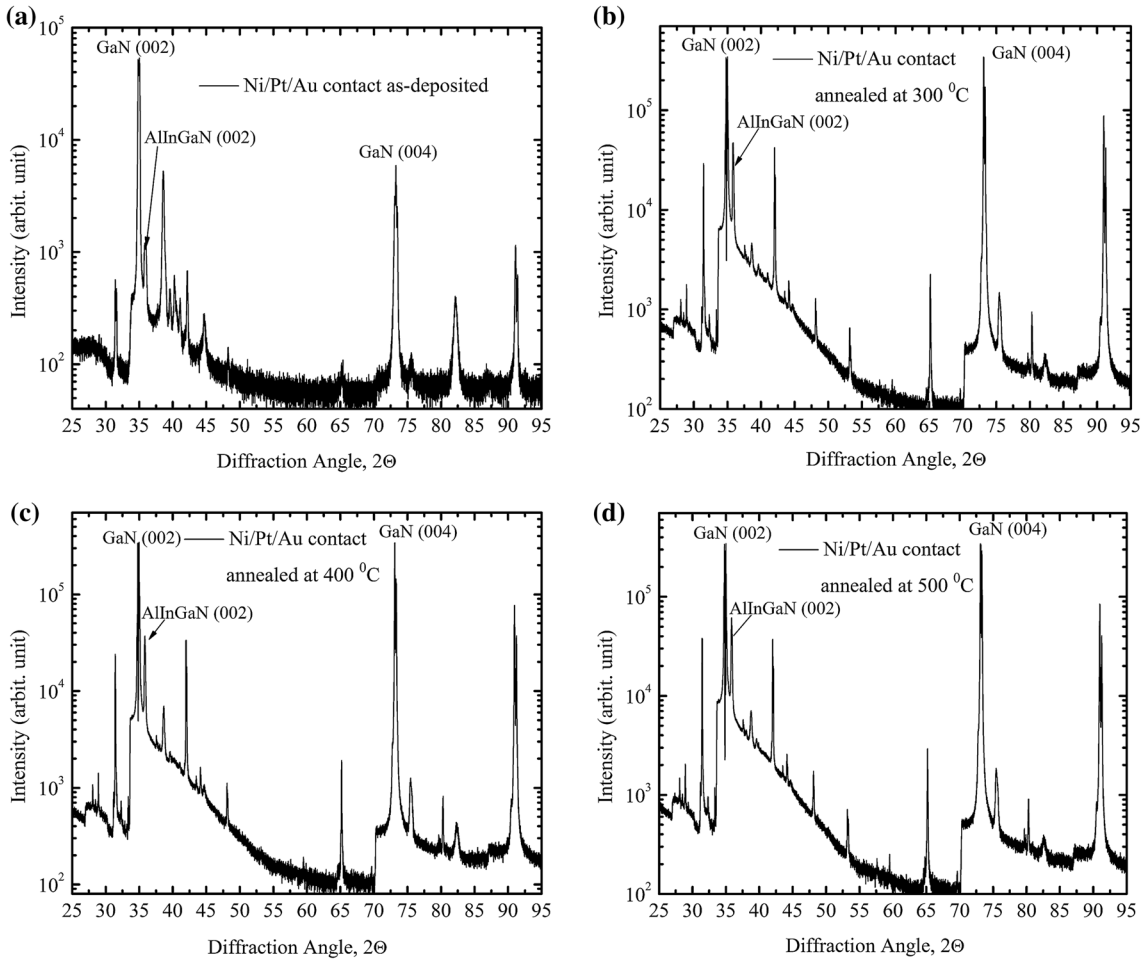


Fig. 5. The x-ray powder diffraction pattern of Ni/Pt/Au Schottky contact on the quaternary $Al_{0.84}In_{0.13}Ga_{0.03}N$ epilayer (a) as-deposited and annealed at (b) 300°C, (c) 400°C, and (d) 500°C.

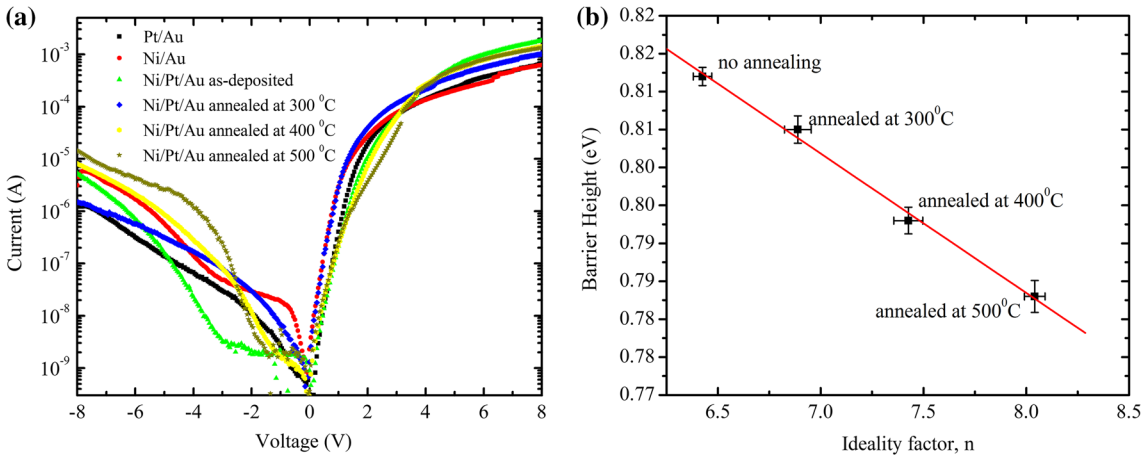


Fig. 6. (a) The forward and reverse bias *I–V* characteristics for the as-deposited Pt/Au, Ni/Au, Ni/Pt/Au Schottky contacts and Ni/Pt/Au Schottky contacts on the quaternary $Al_{0.84}In_{0.13}Ga_{0.03}N$ epilayer annealed at different temperatures. (b) The barrier height versus ideality factor behavior for the as-deposited and annealed at 300°C, 400°C, and 500°C Ni/Pt/Au Schottky contacts are given.

contacts on the quaternary AlInGaN epilayer. The highest SBH was obtained for the Pt/Au (0.82 eV from *I–V*) contacts when they were compared with the as-deposited Schottky contacts. The annealing effect on the SBH of the Ni/Pt/Au Schottky contact on the quaternary AlInGaN epilayer was calculated

**Table I. The experimental values of $I_s$, $n$, $\Phi_{B0}$ (obtained from the *I–V*, Norde, and *C–V* methods), $R_s$ and $R_{sh}$ of Pt/Au, Ni/Au, and Ni/Pt/Au Schottky contacts on quaternary $Al_{0.84}In_{0.13}Ga_{0.03}N$ epilayers and annealing effects on these parameters for Ni/Pt/Au Schottky contacts are listed**

| Schottky contact | Annealing | Saturation currents, $I_s$ (nA) | Ideality factor, $n$ | Barrier heights, $\Phi_{B0}$ (eV) obtained from | | | Series resistance $R_s$ (kΩ) | Shunt resistances $R_{sh}$ (kΩ) |
|---|---|---|---|---|---|---|---|---|
| | | | | *I–V* | *Norde* | *C–V* | | |
| Pt/Au | No | 0.45 ± 0.01 | 5.69 ± 0.04 | 0.82 ± 0.02 | 0.83 ± 0.02 | 1.09 ± 0.01 | 12.40 ± 0.09 | 6530 ± 10 |
| Ni/Au | No | 0.59 ± 0.02 | 6.09 ± 0.05 | 0.82 ± 0.01 | 0.77 ± 0.01 | 1.09 ± 0.02 | 12.70 ± 0.13 | 2550 ± 12 |
| Ni/Pt/Au | No | 0.70 ± 0.03 | 6.42 ± 0.04 | 0.81 ± 0.01 | 0.88 ± 0.02 | 1.08 ± 0.01 | 4.39 ± 0.32 | 1520 ± 7 |
| Ni/Pt/Au | 300°C | 0.93 ± 0.03 | 6.89 ± 0.03 | 0.80 ± 0.02 | 0.79 ± 0.01 | 1.07 ± 0.01 | 7.89 ± 0.27 | 5360 ± 5 |
| Ni/Pt/Au | 400°C | 1.48 ± 0.03 | 7.43 ± 0.06 | 0.79 ± 0.02 | 0.86 ± 0.02 | 1.06 ± 0.02 | 5.65 ± 0.28 | 990 ± 3 |
| Ni/Pt/Au | 500°C | 2.18 ± 0.04 | 8.041 ± 0.05 | 0.78 ± 0.02 | 0.84 ± 0.01 | 1,04 ± 0.01 | 5.98 ± 0.35 | 550 ± 6 |

using the *I–V*, Norde, and *C–V* methods. It is noted that the barrier height decreases with an increase in the annealing temperature up to 500°C compared to that of the as-deposited Ni/Pt/Au Schottky contact. The estimated SBH of the annealed Ni/Pt/Au Schottky contacts, calculated from the *I–V* results, were 0.80 eV, 0.79 eV, and 0.78 eV at 300°C, 400°C, and 500°C, respectively. It is observed that the SBH of the Ni/Pt/Au decreased when the contact was annealed at 500°C. The variation in the barrier height of Ni/Pt/Au Schottky contact after annealing suggests that Ni/Pt/Au metals react with the AlInGaN epilayers, as confirmed by XRD results.

On the other hand, higher ideality factors values were obtained for as-deposited Pt/Au (5.69), Ni/Au(6.09), Ni/Pt/Au (6.42) Schottky contacts and annealed Ni/Pt/Au (6.42) Schottky contacts at 300°C (6.89), 400°C (7.43), and 500°C (8.04). The $n$ values of the Schottky contacts on the quaternary AlInGaN epilayer are much greater than 1. The higher $n$ values can be attributed to the current-transport mechanisms other than thermionic emission, such as dislocation-related tunneling similar to AlGaN[41] and AlInN[14] ternary alloys. In addition, the nitride based alloy is a random alloy; it is subject to a percolation threshold, above which an infinitely connected network of the minority alloy component exists. Because of these, there can be alloy composition inhomogeneity in the small length scales. The alloy composition inhomogeneity inherent to low-temperature nitride-based alloys result in a Schottky barrier height inhomogeneity.[41] Such fluctuations have a significant impact on Schottky barrier performance and can cause a high ideality factor of the Schottky contact on the nitride-based alloys.[42]

The Fig. 6b shows the calculated $\Phi_{B0}$ versus $n$ values of as-deposited and annealed Ni/Pt/Au Schottky contacts. There is a linear correlation between $\Phi_{B0}$ and $n$.

Both the values of series resistance ($R_s$) and shunt resistance ($R_{sh}$) can cause a serious error in the extraction of *I–V* characteristics and they can be extracted from the structure resistance ($R_i$) as a function of applied bias voltage ($V_i$) by using Ohm's Law ($R_i = dV/dI$). However, the real values of $R_s$ and $R_{sh}$ for these contacts correspond to enough high forward and reverse bias voltages as seen in Fig. 7. As can be seen in Fig. 7 and Table I, both the values of $R_s$ and $R_{sh}$ are a function of bias voltage and changed from range to range due to a particular distribution of surface charges, barrier, and interfacial layer inhomogeneities.

The high series resistance across the Schottky contact can inhibit accurate evolution of barrier height from the standard ln *I–V* plot. For this case, the Norde method makes it convenient to calculate the values of $R_s$ and $\Phi_{B0}$ by considering Eq. 1 in the situation where the voltage across the diode is greater than 3kT/q.[43] In this method, a function $F(V)$ is plotted against voltage[44]:

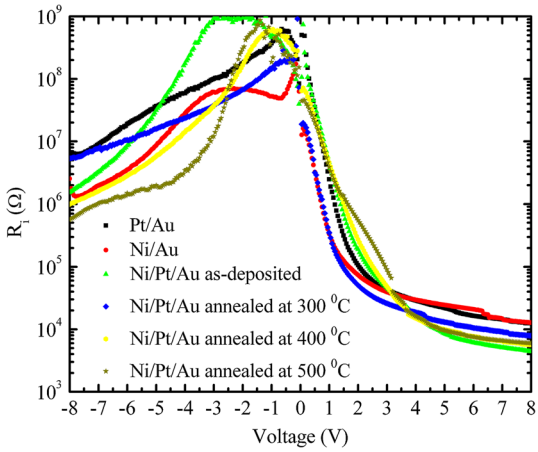


Fig. 7. The profile of the structure resistance ($R_i$) versus $V_i$ plots for the as-deposited Pt/Au, Ni/Au, Ni/Pt/Au Schottky contacts and Ni/Pt/Au Schottky contacts on the quaternary $Al_{0.84}In_{0.13}Ga_{0.03}N$ epilayer annealed at different temperatures.

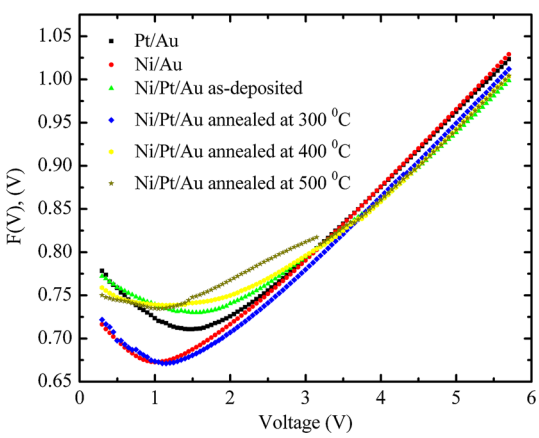


Fig. 8. Modified Norde plot, obtained from forward *I–V* characteristics at room temperature, for the as-deposited Pt/Au, Ni/Au, Ni/Pt/Au Schottky contacts and Ni/Pt/Au Schottky contacts on the quaternary $Al_{0.84}In_{0.13}Ga_{0.03}N$ epilayer annealed at different temperatures.

$$F(V) = \frac{V}{\gamma} - \frac{kT}{q}\ln\left(\frac{I(V)}{AA^{*}T^{2}}\right) \tag{3}$$

Here, $I$ is the current and the integer denoted by $\gamma$ is also greater than the $n$ value. $F(V)$–$V$ plots (Fig. 8) have minimum points of $V_{min}$ and $I_{min}$ which are used to calculate the values of $R_s$ and $\Phi_{B0}$ by Eqs. 4a and 4b, respectively.

$$R_s = \frac{(\gamma - n)kT}{qI_{min}}, \tag{4a}$$

$$\Phi_{B0} = F(V_{min}) + \frac{V_{min}}{\gamma} - \frac{kT}{q} \tag{4b}$$

The obtained experimental values of the $F_{min}$, $V_{min}$, $I_{min}$, $R_s$ and $\Phi_{B0}$ (in Table I) obtained from the Norde function are tabulated in Table II for each Schottky contact. As can be seen in Tables I and II, the $R_s$ values obtained from Ohm's Law and Norde method are usually closer to each other, but some discrepancies in the values of $R_s$ can be attributed to the nature of the measurement methods corresponding to different voltages.

Figure 9a and b shows the $C$–$V$ and $G/\omega$–$V$ behavior of the as-deposited Pt/Au, Ni/Au, Ni/Pt/Au Schottky contacts and annealed Ni/Pt/Au Schottky contacts on a quaternary $Al_{0.84}In_{0.13}Ga_{0.03}N$ epilayer measured bias voltage between − 8 V and 8 V and frequency of 500 kHz at room temperature. It is clear that both the $C$–$V$ and $G/\omega$–$V$ plots exhibit reverse, depletion, and accumulation regions for each diode.

The doping profile of the semiconductor (both $n$-type and $p$-type) and the barrier height $\Phi_B(C\text{–}V)$ of a metal–semiconductor rectifying contact or Schottky barrier diodes can be calculated using a $C$–$V$ (capacitance versus voltage) measurement.[38,39,43] In the $C$–$V$ technique, a small AC signal is usually superimposed on the DC bias voltage so that charges of one sign are induced on the metal surface and the charges of the opposite sign on the semiconductor.[38,39,43] Thus the field-ionized impurity concentration in the semiconductor depletion region can be calculated by measuring the capacitance as a function of the DC bias voltage. For Schottky type contacts, the value of capacitance in a depletion layer can be expressed as[38,39,44];

$$\frac{1}{C^2} = \frac{2}{q\varepsilon_s\varepsilon_o N_A A^2}\left(V_D - \frac{kT}{q} - V_R\right) \tag{5}$$

In Eq. 5, $\varepsilon_s$ is the permittivity of the semiconductor, $\varepsilon_o$ is the permittivity of free space, $N_D$ is the doping concentration of donor atoms, $V_D$ is the diffusion potential and $V_R$ is the reverse bias voltage. The permittivity values for the $Al_{0.84}In_{0.13}Ga_{0.3}N$ epilayer were estimated as 12.3 by a linear extrapolation from the measured values of AlN, InN, and GaN.[40] The values of $V_D$ and $N_D$ are obtained from the intercept and slope of the linear part of $C^{-2}$ versus $V$ plots, respectively[39,44];

$$N_D = \frac{2}{q\varepsilon_s\varepsilon_0 A^2 \tan\theta} \tag{6a}$$

Thus, the value of Fermi energy ($E_F$) for the Schottky contacts using the equation below[39];

$$E_F = \frac{kT}{q}\ln\left(\frac{N_c}{N_D}\right) \tag{6b}$$

with

$$N_c = 2\left[\frac{2\pi m_e^* kT}{h^2}\right]^{3/2} \tag{7}$$

where $N_c$ is the effective density of states in the conductance band of the semiconductor and $m_e^*$ is

**Table II. The values of $F_{min}$, $V_{min}$, $I_{min}$ and $R_s$ calculated from Norde function for the Schottky contacts on quaternary $Al_{0.84}In_{0.13}Ga_{0.03}N$ epilayer at room temperature**

| Schottky contact | Annealing | $F_{min}$ (V) | $V_{min}$ (V) | $I_{min}$ ($\mu$A) | $R_s$ (kΩ) | $R_s$ (C/G–V) (kΩ) |
|---|---|---|---|---|---|---|
| Pt/Au | No | 0.685 | 1.448 | 3.91 | 27.62 ± 0.12 | 3.13 ± 0.18 |
| Ni/Au | No | 0.673 | 0.998 | 2.90 | 33.71 ± 0.21 | 3.46 ± 0.22 |
| Ni/Pt/Au | No | 0.73 | 1.548 | 2.71 | 33.04 ± 0.18 | 1.45 ± 0.16 |
| Ni/Pt/Au | 300°C | 0.671 | 1.148 | 5.73 | 13.62 ± 0.26 | 2.65 ± 0.15 |
| Ni/Pt/Au | 400°C | 0.739 | 1.198 | 0.49 | 13.28 ± 0.31 | 1.85 ± 0.32 |
| Ni/Pt/Au | 500°C | 0.735 | 1.048 | 0.32 | 15.45 ± 0.17 | 2.04 ± 0.25 |

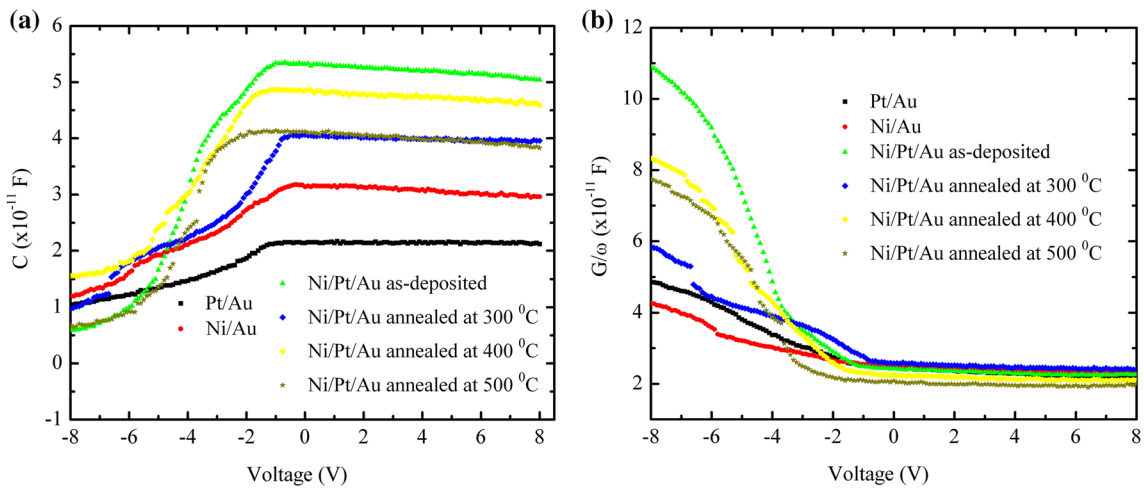


Fig. 9. The reverse and forward bias (a) *C–V* and (b) *G/ω–V* characteristics, measured at room temperature, for the as-deposited Pt/Au, Ni/Au, Ni/Pt/Au Schottky contacts and Ni/Pt/Au Schottky contacts on the quaternary $Al_{0.84}In_{0.13}Ga_{0.03}N$ epilayer annealed at different temperatures.

the effective mass of the electron. Thus, the value of barrier height $\Phi_B(C–V)$ was calculated using the value of voltage intercept $V_o$ for each Schottky contact in the relation below:

$$\phi_B(C-V) = \left(V_0 + \frac{kT}{q}\right) + E_F = V_D + E_F \quad (8)$$

The obtained experimental values of the $\Phi_B(C–V)$ are also given in Table I. As shown in Table I, the value of SBH obtained from the reverse bias *C–V* characteristics is higher than the forward bias *I–V* characteristics due to the nature of measurements method for each sample. Under the reverse bias condition, the total electric field (interior and external) and depletion layer width are higher than forward biases.

The voltage dependent value of $R_s$ for each sample was also extracted from the measured *C* and *G* values by using Niccolian and Brews. According to this method, the accurate value of $R_s$ can be extracted from the *C* and *G* values at the strong accumulation region, but it can also be extracted as a function of applied bias voltage as the following equation[44]:

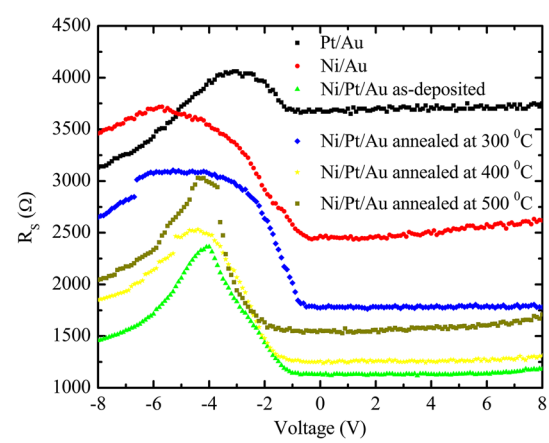


Fig. 10. The $R_s$–*V* plots obtained from the C/G–V data of the as-deposited Pt/Au, Ni/Au, Ni/Pt/Au Schottky contacts and Ni/Pt/Au Schottky contacts on the quaternary $Al_{0.84}In_{0.13}Ga_{0.03}N$ epilayer annealed at different temperatures at room temperature.

$$R_s = \frac{G_m}{G_m^2 + (\omega C_m)^2} \quad (9)$$

Figure 10 shows the voltage dependent profile of $R_s$ for each contact at room temperature. As shown in

Tables I and II, values of $R_s$ using obtained from Norde function, Ohm's Law from *I–V* data and Nicollian-Brews method from *C–V* and $G/\omega$–*V* data almost match each other.

## CONCLUSIONS

In the present study, the Schottky contact parameters of the Pt/Au, Ni/Au, Ni/Pt/Au contacts on the quaternary $Al_{0.84}In_{0.13}Ga_{0.03}N$ epitaxial layer and thermal annealing effects on the electrical and structural properties of the Ni/Pt/Au contacts were investigated by *I–V*, *C–V* and *XRD* measurements. The higher ideality factors values were obtained for as-deposited Pt/Au (5.69), Ni/Au (6.09), Ni/Pt/Au (6.42) Schottky contacts and annealed Ni/Pt/Au (6.42) Schottky contacts at 300°C (6.89), 400°C (7.43), and 500°C (8.04). The higher $n$ results can be attributed to the current-transport mechanisms other than thermionic emission, such as dislocation related tunneling.

The highest SBH was obtained for the Pt/Au (0.82 eV (*I–V*), 0.83 (Norde), and 1.09 (*C–V*)) contacts when they were compared with the other as-deposited Schottky contacts. On the other hand, the estimated SBH of the Ni/Pt/Au Schottky contacts decreases with an increase in the annealing temperature (from *I–V* results; 0.80 eV(300°C), 0.79 eV(400°C), and 0.78 eV(500°C)). The variation in the barrier height of Ni/Pt/Au Schottky contact after annealing suggests that Ni/Pt/Au metals react with the $Al_{0.84}In_{0.13}Ga_{0.03}N$ epilayers, as confirmed by the XRD results.

## ACKNOWLEDGMENTS

This work is supported by TUBITAK under Project No. 116F041. One of the authors (E.O.) also acknowledges partial support from the Turkish Academy of Sciences.

## REFERENCES

1. M.E. Levinshtein, S.L. Rumyantsev, and M.S. Shur, *Properties of Advanced Semiconductor Materials: GaN, AIN, InN, BN, SiC, SiGe* (New York: Wiley, 2001). ISBN 978-0-471-35827-5.
2. R.S. Pengelly, S.M. Wood, J.W. Milligan, S.T. Sheppard, and W.L. Pribble, *IEEE Trans. Microw. Theory Tech.* 60, 1764 (2012).
3. S. Nakamura, *Science* 281, 956 (1998).
4. N. Ketteniss, L.R. Khoshroo, M. Eickelkamp, M. Heuken, H. Kalisch, R.H. Jansen, and A. Vescan, *Semicond. Sci. Technol.* 25, 075013 (2010).
5. T. Lim, R. Aidam, P. Waltereit, T. Henkel, R. Quay, R. Lozar, T. Maier, L. Kirste, and O. Ambacher, *IEEE Electron. Dev. Lett.* 31, 671 (2010).
6. H. Hirayama, *J. Appl. Phys.* 97, 091101 (2005).
7. R. Wang, G. Li, J. Verma, B.S. Rodriguez, T. Fang, J. Guo, Z. Hu, O. Laboutin, Y. Cao, W. Johnson, G. Snider, P. Fay, D. Jena, and H. Xing, *IEEE Electron. Dev. Lett.* 32, 1215 (2011).
8. B. Reuters, A. Wille, B. Hollander, E. Sakalauskas, N. Ketteniss, C. Mauder, R. Goldhahn, M. Heuken, H. Kalisch, and A. Vescan, *J. Electron. Mater.* 41, 905 (2012).
9. B. Reuters, A. Wille, N. Ketteniss, H. Hahn, B. Hollander, M. Heuken, H. Kalisch, and A. Vescan, *J. Electron. Mater.* 42, 826 (2013).
10. S.L. Rumyantsev, N. Pala, M.S. Shur, R. Gaska, M.E. Levinshtein, M. Asif Khan, G. Simin, X. Hu, and J. Yang, *J. Appl. Phys.* 88, 6726 (2000).
11. S. Karboyan, J.G. Tartarin, M. Rzin, L. Brunel, A. Curutchet, N. Malbert, N. Labat, D. Carisetti, B. Lambert, M. Mermoux, E. Romain-Latu, F. Thomas, C. Bouexière, and C. Moreau, *Microelectron. Reliab.* 53, 1491 (2013).
12. D. Marcon, T. Kauerauf, F. Medjdoub, J. Das, M. Van Hove, P. Srivastava, K. Cheng, M. Leys, R. Mertens, S. Decoutere, G. Meneghesso, E. Zanoni, and G. Borghs, in *IEEE International Electron Devices Meeting*, 20.3.1, 2010.
13. F. Lee, L.-Y. Su, C.-H. Wang, Y.-R. Wu, and J. Huang, *IEEE Electron. Dev. Lett.* 36, 232 (2015).
14. E. Arslan, Ş. Altındal, S. Özçelik, and E. Ozbay, *Semicond. Sci. Technol.* 24, 075003 (2009).
15. J. Ren, D. Yan, G. Yang, F. Wang, S. Xiao, and X. Gu, *J. Appl. Phys.* 117, 154503 (2015).
16. A. Kumar, M. Latzel, S. Christiansen, V. Kumar, and R. Singh, *Appl. Phys. Lett.* 107, 093502 (2015).
17. Y. Koyama, T. Hashizume, and H. Hasegawa, *Solid-State Electron.* 43, 1483 (1999).
18. E. Monroy, F. Calle, R. Ranchal, T. Palacios, M. Verdu, F.J. Sanchez, M.T. Montojo, M. Eickhoff, F. Omnes, Z. Bougrioauand, and I. Moerman, *Semicond. Sci. Technol.* 17, L47 (2002).
19. S. Arulkumaran, T. Egawa, H. Ishikawa, M. Umeno, and T. Jimbo, *IEEE Trans. Electron. Dev.* 48, 573 (2001).
20. L. Fang, S. Bo, L. Li-Wu, M. Nan, X. Fu-Jun, M. Zhen-Lin, S. Jie, L. Xin-Yu, W. Ke, and H. Jun, *Chin. Phys. B* 19, 127304 (2010).
21. J. Pedrós, R. Cuerdo, R. Lossy, N. Chaturvedi, J. Würf, and F. Calle, *Phys. Status Solidi (C)* 3, 1709 (2006).
22. S. Kim, H.J. Kim, S. Choi, J.-H. Ryou, R.D. Dupuis, K.-S. Ahn, and H. Kim, *Jpn. J. Appl. Phys.* 52, 10MA05 (2013).
23. R. Khanna, S.J. Pearton, F. Ren, and I. Kravchenko, *Appl. Surf. Sci.* 252, 5814 (2006).
24. V.R. Reddy, M. Ravinandan, P. Koteswara Rao, and C.-J. Choi, *J. Mater. Sci. Mater. Electron.* 20, 1018 (2009).
25. J. Wang, D.G. Zhao, Y.P. Sun, L.H. Duan, Y.T. Wang, S.M. Zhang, H. Yang, S. Zhou, and M. Wu, *J. Phys. D Appl. Phys.* 36, 1018 (2003).
26. T.N. Order, P. Martin, J.Y. Lin, H.X. Jiang, J.R. Williams, and T. Isaacs-Smith, *Appl. Phys. Lett.* 88, 183505 (2006).
27. N. Miura, T. Nanjo, M. Suita, T. Oishi, Y. Abe, T. Ozeki, H. Ishikawa, T. Egawa, and T. Jimbo, *Solid-State Electron.* 48, 689 (2004).
28. K.J. Reddy, V.R. Reddy, and E.P.N. Reddy, *J. Mater. Sci. Mater. Electron.* 19, 333 (2008).
29. A. Akkaya, L. Esmer, B.B. Kantar, H. Çetin, and E. Ayyıldız, *Microelectron. Eng.* 130, 62 (2014).
30. G. Greco, F. Iucolano, S.D. Franco, C. Bongiorno, A. Patti, and F. Roccaforte, *IEEE Trans. Electron. Dev.* 63, 2735 (2016).
31. Y. Liu, H. Jiang, T. Egawa, B. Zhang, and H. Ishikawa, *J. Appl. Phys.* 99, 123702 (2006).
32. M.A. Laurent, G. Gupta, D.J. Suntrup III, S.P. DenBaars, and U.K. Mishra, *J. Appl. Phys.* 119, 064501 (2016).
33. Y. Liu, T. Egawa, H. Jiang, B. Zhang, H. Ishikawa, and M. Hao, *Appl. Phys. Lett.* 85, 6030 (2004).
34. A.J. Ghazai, H.A. Hassan, Z. Hassan, and A.S. Hussein, *Optoelectron. Adv. Mater. Rapid Commun.* 6, 324 (2012).
35. M. Gökçen and M. Yıldırım, *Chin. Phys. B* 21, 128502 (2012).
36. K. Akkılıç, A. Türüt, G. Cankaya, and T. Kılıçoğlu, *Solid-State Commun.* 125, 551 (2003).
37. E. Arslan, S. Bütün, Y. Şafak, H. Uslu, İ. Taşçıoğlu, Ş. Altındal, and E. Özbay, *Microelectron. Reliab.* 51, 370 (2011).
38. H. Card and E. Rhoderick, *J. Phys. D Appl. Phys.* 4, 1589 (1971).
39. S.M. Sze and K.K. Ng, *Physics of Semiconductor Devices*, 3rd ed. (Hoboken: Wiley, 2006).
40. H. Morkoç, *Handbook of Nitride Semiconductors and Devices*, Vol. 1 (Weinheim: Wiley, 2008). ISBN 978-3-527-40837-5.

41. S. Zhang, B. Liu, J.Y. Yin, H.H. Sun, Z.H. Feng, and L.C. Zhao, *J. Phys. D Appl. Phys.* 44, 075405 (2011).
42. N. Nanda, K. Reddy, and V. Rajagopal Reddy, *Bull. Mater. Sci.* 35, 53 (2012).
43. E. Arslan, Ş. Altındal, S. Özçelik, and E. Özbay, *J. Appl. Phys.* 105, 023705 (2009).
44. E.H. Nicollian and J.R. Brews, *Metal Oxide Semiconductor (MOS) Physics and Technology* (New York: Wiley, 1982).